JOINT EUROPEAN TORUS

JET–P(90)55

F.B. Marcus, J.M. Adarns, A.D. Cheetharn, S. Conroy, W.G.F. Core, O.N. Jarvis,
M.J. Loughlin, M. Olsson, G. Sadler, P. Smeulders, P. van Belle,
N. Watkins and JET Team

JET Neutron Emission Profiles and Fast Ion Redistribution during Sawtooth Crashes

JET Neutron Emission Profiles and Fast Ion Redistribution during Sawtooth Crashes

F.B. Marcus, J.M. Adarns[1], A.D. Cheetharn[2], S. Conroy, W.G.F. Core, O.N. Jarvis, M.J. Loughlin, M. Olsson[3], G. Sadler, P. Smeulders, P. van Belle, N. Watkins and JET Team*

JET-Joint Undertaking, Culham Science Centre, OX14 3DB, Abingdon, UK

[1]AEA Industrial Technology, Harwell Laboratory, Didcot,OXll ORA
[2]Present Address: Canberra University, Canberra, Australia
[3]Royal Institute of Technology, Stockholm, Sweden
** See Appendix 1*

Preprint of Paper to be submitted for publication in
Plasma Physics and Controlled Fusion

JET NEUTRON EMISSION PROFILES AND FAST ION REDISTRIBUTION DURING SAWTOOTH CRASHES*

F B Marcus, J M Adams[1], A D Cheetham[2], S Conroy, W G F Core, O N Jarvis, M J Loughlin, M Olsson[3], G Sadler, P Smeulders, P van Belle, N Watkins[1]

JET Joint Undertaking, Abingdon, Oxfordshire OX14 3EA, UK
[1]AEA Industrial Technology, Harwell Laboratory, Didcot, OX11 ORA, UK
[2]Present address:Canberra University, Canberra, Australia
[3]Royal Institute of Technology, Stockholm, Sweden

ABSTRACT

Measurements from the JET neutron profile monitor are analysed tomographically to deduce the 2-D spatial distribution of neutron emissivity during NBI heating both before and after sawtooth crashes. In a discharge where the global neutron emission decreases slightly to 5/6 of the pre-crash rate of nearly 10^{16} n/s, the axial emissivity drops much more to only 1/6 of the pre-crash value. The sources of neutron emissivity are analysed with an analytic Fokker-Planck formulation. The main change in neutron emissivity is due to fast ion redistribution during a sawtooth crash and a decrease in beam-beam produced emissivity. The deduced fast ion redistribution is consistent with other observations on sawtooth behaviour in JET.

*This paper is an expanded version of a presentation contributed to the 17th EPS Plasma Physics Division Conference, Amsterdam, The Netherlands, June 1990

1. INTRODUCTION

At the JET tokamak and other large nuclear fusion experiments such as TFTR, a major goal is the production and measurement of high levels of neutron emission from d-d and, ultimately, d-t fusion reactions. A variety of neutron diagnostics as exploited by JARVIS et al. (1990) has been used independently at JET to measure both fast and thermal ion behaviour. In conjunction with other plasma diagnostics, the parameters of the thermal plasma and fast ions created by neutral beam or radio frequency heating can be derived. The available neutron diagnostics include global emission detectors, spectrometers and (the main subject of this paper) a neutron profile monitor consisting of a vertical and horizontal camera. The profile monitor measures collimated line-integral neutron emission, which allows the unfolding of neutron emissivity spatial profiles in two dimensions. These profiles are used to study the thermal and beam-induced sources of neutron emission and to analyse the fast ion redistribution due to sawtooth crashes. The deuteron distribution function in velocity space is a combination of a thermal plasma and a deuterium beam slowing down distribution. The interactions of ions within this combined distribution result in d-d fusion which produces neutrons near 2.45 MeV. We consider the sources of neutron production in terms of the self-interactions of the thermal and beam distributions (thermal and beam-beam) and cross-interactions (beam-plasma).

To classify and understand the effects of sawtooth crashes on the global neutron emission and local emissivity, we need to consider the sources and amplitudes of neutron emission (thermal, beam-plasma, beam-beam, rf-induced), the sources of ion and electron heating (ohmic, beams, rf), the magnetic configuration, plasma profiles (density, temperature, fast ion, and current), type of instability, fast ion stabilization, etc. Over the years, sawteeth have been observed in the global neutron emission from tokamaks and attempts have been made to connect them with models of electron sawteeth, for example: MARCUS et al. (1983), PFEIFFER et al. (1985), LOVBERG et al. (1989), and BATISTONI et al. (1990). The main restriction on previous analyses has been that neutron profile data has not been available. In the present paper, we use the JET neutron profile monitor to study the profiles before and after a sawtooth crash on a sufficiently rapid time scale to study the redistribution of fast ions. This profile information allows us to

compare the experimental information with other observations of sawteeth in JET, as described by CAMPBELL et al. (1988).

2. INSTRUMENTAL DETAILS AND DATA ANALYSIS METHODS

The neutron profile monitor described by ADAMS et al. (1989) is shown in Fig. 1 with the lines-of-sight delineated. It consists of: 2 heavy-concrete (3000 kg/m^3) fan-shaped multi-collimator cameras with 10 horizontal channels and 9 vertical channels (8 are used here, since the innermost channel #11 has excessive gamma ray count-rates) and NE-213 scintillators to detect 2.45 MeV neutrons. The scintillators are operated with pulse shape discrimination of neutrons and gamma rays, and a lower energy detection bias of 2 MeV to reject scattered neutrons.

The raw data are corrected for neutrons back-scattered from material in the lines-of-sight, detector live time, detection efficiency, neutron attenuation, collimator scattering and collimator solid angles.

The viewing width in the poloidal plane is 0.1 m in the central channels and 0.2 m in the edge channels. The channel separation is 0.2 m in the central plasma region. The channel-to-channel efficiency has a systematic error of about 10%. To obtain a statistical error of less than 10% requires a global emission of 10^{16} n/s for 10 ms, or correspondingly longer times at lower emission rates to achieve sufficient counts in the channels viewing significant neutron emission.

Neutron emissivity profiles in 1-D have previously been unfolded from profile monitor measurements using the program "ORION" produced by CONROY (1990) and employed by ADAMS et al (1989), which uses flux surfaces from MHD equilibrium and assumes them to be surfaces of constant neutron emission. A best fitting curve is generated by an analytical source function with a small number of free parameters. The plasma neutron emissivity has also been calculated *a priori* in the 2-D plasma transport code "TRANSP", as discussed by SADLER et al. (1990). The result is integrated along the profile monitor's lines-of-sight and agrees acceptably with the experimental data.

In this paper, constrained tomography as discussed by GRANETZ et al. (1988) is used to determine the 2-D neutron emissivity profile from the line-integral measurements. A standard geometry is chosen for the inversion which consists of nested elliptical surfaces with a fixed ellipticity of 1.5 centred on R = 3.02 m and Z = 0.0 m, with a maximum horizontal minor radius of 1.0 m. The deduced shape of the emissivity profile is relatively independent of this geometry. The profile can have a different centre than the standard geometry and varying

elongation and shape. Near-elliptic contours described by a 4-term Fourier expansion poloidally and radial Abel inversion are employed for the tomographic analysis. The lines-of-sight are assumed to be of zero width in the analysis program, which is a good approximation for profiles without too strong a channel-to-channel variation. The analysis program initially smoothes the measured channel data into synthesized 100-channel signals for each camera before the inversions are performed, to avoid unphysical oscillations in the tomographic solution. Further smoothing is performed during the tomographic inversion. The amount of smoothing is chosen so that the deduced emissivity profile gives line-integrals which are within one standard deviation of the original experimental measurements.

Given these limitations, the amount of fine structure detail obtainable is very limited. Tests using model profiles generated by the "ORION" code and including 10% random errors show that peaked, flat, hollow, double humped, and outwardly shifted profiles, when reconstructed by 2-D tomography, can be distinguished from each other. The correct emissivity values can be calculated. The advantages of 2-D tomography not constrained by geometry are that emissivity profiles may be found which were not guessed *a priori*, and that departures from constant emission on a flux surface may be observed.

To demonstrate the method and to find the shape of the neutron emissivity profile just before a sawtooth crash, we examine Discharge 20981, which has a high rate of neutron production, during a time interval of 10 ms from 10.738 s - 10.748 s. We will subsequently compare this profile with the profile after the crash.

In Fig. 2, the experimental channel data (numbers) from the two neutron cameras, measuring the line-integrals of the neutron emissivity, are compared to curves (one for each camera) of line-integrals calculated by integrating the inverted profiles to reproduce the expected signal. The deduced curves appear smooth since the tomography assumes that each camera has 100 channels. The horizontal axis in Fig. 2 is the position of the intersection of the ellipse in the standard solution geometry (see above) tangent to the camera with the horizontal major radius.

In Fig. 3, the neutron emissivity profile deduced by tomography is shown as a function of major radius and vertical height. The neutron emissivity is strongly peaked on axis, with a maximum value of 1.9×10^{15} $m^{-3}s^{-1}$. By observing the emissivity versus position on a

major radius chord passing through the axis, a Full-Width-Half-Maximum (FWHM) of 0.36 m is measured at the mid-plane. In the rest of the paper, this geometric convention for determining the FWHM will be maintained.

To examine the global validity of the data, 34 time slices on several discharges were analysed to find the neutron emissivity in two dimensions, using the tomography method. The emissivity was integrated to find the global emission, referred to as E_t in Fig. 4; this is compared to the calibrated geometry-corrected global emission measured by the fission chambers, referred to as E_f in Fig. 4. Absolutely calibrated fission chambers on JET measure the total neutron emission rate to 7% accuracy. The ratio E_t/E_f is plotted against E_f over 5 decades of emission, from 10^{12} up to 3 x 10^{16} n/s. The best fit to the data with a linear scaling is:

$$E_t/E_f = [\ 0.96 + 0.13 * (E_f / 10^{16})\ ] \pm 0.06$$

As seen in Fig. 4, the ratio is nearly constant at about 1.0 up to global rates of 10^{16} n/s, and starts to deviate above this level, where neutron count rates begin to exceed 100 kHz in individual spectrometer channels.

Some modest variation of the E_t/E_f ratio with the global emission is expected from at least two sources, based on calculations with a code described by VAN BELLE and SADLER (1986): (i) as additional heating is supplied and T_i increases, there is an upward shift of neutron energy which leads to an increase in detection efficiency (< 5% in reasonable conditions) by the profile monitor; (ii) for beam heating (or any heating involving deuteron ion anisotropy), the anisotropy of the d-d reaction leads to preferential radial emission of neutrons (10% increase in extreme beam-beam cases). The rapid deviation above 10^{16} n/s is unphysical and is attributed to pile-up of gamma-ray events being recorded erroneously as neutron events. For neutron emission rates above 10^{16} n/s, more accurate profiles are obtained by eliminating channels with excessive count rates from the fitting procedure. This restricted procedure at high count rate reduces the ratio, but gives less accurate profile shapes.

In the absence of sawteeth and high plasma density, neutron emissivity profiles are peaked on axis. The FWHM of the emissivity is

much less than the plasma diameter. However, with high plasma density and beam injection, emissivity profiles broaden and shift outwards, as seen by LOUGHLIN et al. (1989). This shift is shown in Fig. 5 by the response of the line-integral measurement of the emissivity by the channels in the vertical neutron camera. The outward shift in emissivity occurs as the density increases with time. The neutral beam deposition also moves towards larger major radius as the density increases. Beam ions deposited at large major radius are further localized in trapped orbits. A detailed comparison between expected and measure neutron emissivity due to these beams is a subject for future investigations.

3. SAWTOOTH CRASHES AND RESPONSE OF THE NEUTRON EMISSIVITY

JET has a wide range of heating methods, plasma profiles and ratios of beam-beam, beam-plasma, and thermal neutron emission. In beam-plasma dominated discharges, a sawtooth crash can cause almost no change in the global neutron emission, but it produces a major redistribution of the emissivity profile. In discharges where thermal neutron emission dominates (Ohmic and RF), a sawtooth crash can cause a large fall in global emission and an even larger fall in the central emissivity. This behaviour is also observed in discharges with high toroidal beta (the ratio of plasma to toroidal magnetic field pressure). In what follows, we investigate discharges with relatively high neutron yields. We also consider discharges with lower neutron yields, but larger drops in the global neutron yield after the sawtooth crash.

To obtain the best time resolution, a sawtooth occurring when the neutron emission rate is $10^{16}s^{-1}$ is examined in Discharge 20981 at 10.75 s. The discharge is a 4 MA deuterium plasma in the double-null H-mode configuration with deuterium neutral beam heating. The global neutron emission, measured by fission chambers and shown in Fig. 6, falls with a 10 ms sampling rate from $9.1x10^{15}s^{-1}$ to $7.5x10^{15}s^{-1}$, a drop of 1/6. Viewed on a fast time scale, the emission falls in about 0.4 ms, compared to the detector intrinsic time response of about 0.1 ms, including neutron thermalization. The emission recovers to the pre-sawtooth crash value after 50 ms, and then continues to increase to a peak of $3.5x10^{16}s^{-1}$ at 11.4 s. At 70 ms before the sawtooth crash, the electron density and temperature profiles are approximately flat over 1.0 m in the mid-plane with values of $1.6x10^{19}m^{-3}$ and 5.0 keV. The peak ion temperature is about 11 keV. After the crash, the electron temperature profile has widened and the central temperature has dropped by about 1/10. The electron density has remained flat. The soft x-ray emissivity has fallen on axis and has broadened.

The line-integrated neutron emission as measured by the channels of the profile monitor show distinct jumps at sawtooth crashes, within the sampling time of 1 ms. In both the horizontal camera and the vertical camera, the profiles change from very peaked before, to very flat after the sawtooth crash. The response of the horizontal neutron camera channels is shown in Fig. 7, where each time bin of 10 ms has a common vertical scale, with a maximum neutron emission of $6.5x10^{14}m^{-2}s^{-1}$. A flat distribution of line-integrals indicates a hollow emissivity

profile. The profiles evolve slowly for 100 - 200 ms and peak again only after about 300 ms. These times are characteristic of beam slowing down times in the evolving plasma. The new peak is broader than before the sawtooth crash.

The neutron emissivity profiles deduced from tomography are shown for Discharge 20981 in Fig. 3 just before (10.738-10.748 s) and in Fig. 8 just after (10.756-10.766 s) the sawtooth crash. The neutron emissivity before is highly peaked on axis at $1.9 \times 10^{15} m^{-3} s^{-1}$, and the emissivity FWHM is 0.36 m. Emissivity contours are nearly circular on axis and elliptical further out. The profile after the crash is much flatter and broader with a FWHM of 1.2 m, although the global emission has fallen by only 1/6. The poloidally-averaged emissivity inside this region is in the range $2\text{-}3 \times 10^{14} m^{-3} s^{-1}$. This is less than 1/6 of the pre-sawtooth crash values. The line-integrals from these profiles are within 5% of measurements for most channels and 12% for the central channel. The profile can be characterized as hollow plus an axial peak. To fit a flat profile would require much larger error bars of up to 30% for several channels.

An analytic Fokker-Planck formulation from CORE (1985) has been extended to include the velocity space diffusion effects of finite ion temperature. Beam ions diffusing above their injection energy have enhanced fusion reactivity. This formulation is used to calculate the expected fraction of beam-beam (bb), beam-plasma (bp) and thermal (t) contributions to axial neutron emissivity, based on measured plasma parameters and calculated beam deposition profiles. For example, the maximum axial emissivity during Discharge 20981 at 11.4 s is composed of 1/6 bb, 1/2 bp, 1/3 t, with a beam slowing-down time of 130 ms for an 80 keV deuteron.

Analysing the data for the interval immediately preceding the sawtooth crash at 10.75 s, a lower limit for the slowing-down time of injected beam ions is calculated to be 300 ms. The NBI source rate on axis is $10^{20} m^{-3} s^{-1}$, injection has lasted only 260 ms, during which the deuteron density has increased to about $1.7 \times 10^{19} m^{-3}$. The central density is therefore mainly composed of fast ions which have not had time to fully thermalize. The axial neutron emissivity can be accounted for by bb fusion reactions only, using a reaction rate appropriate for beam ions that are only partially thermalized. In the regions off-axis, the fast ion density is lower and the thermal ion fraction higher than on-axis. The bp reactions dominate over bb, while t reactions are at

the 1% level. This general picture is supported with full profile simulations by BALET et al. (1989) in a separate calculation using "TRANSP", where bb dominates on axis, but represents only 1/3 of the global neutron emission.

After the sawtooth crash, the drop of only 1/6 in the total neutron emission and the change in the neutron emissivity profile are consistent with a redistribution of fast ions within the plasma, as observed by SADLER et al. (1989). The bb emission, which previously represented 1/3 of the emission and which is proportional to the square of the fast-ion density, drops with increased volume and is nearly eliminated. The bp emission from most fast ions would be expected to be approximately unchanged, since they are redistributed in a region with relatively uniform electron and, since the impurity content is low, relatively uniform thermal deuteron density. However, the total deuteron density is the sum of the fast and thermal deuteron density, with the fast-ion contribution largest on axis. Fast ions which were previously on axis, when redistributed with thermal ions, would therefore give additional bp reactions, but with a lower reaction rate than from bb in the centre. The net resultant drop is therefore expected to be less than the 1/3 bb contribution before the crash, and is in fact observed to be only a 1/6 drop.

The remaining neutron emission is therefore mostly bp after the sawtooth crash, and the profile evolves slowly on the same time scale as the beam slowing-down time scale. At the same time, newly injected beam ions contribute to the axial neutron emission. Previous JET results on electron temperature sawteeth discussed by CAMPBELL et al. (1988) indicate that a hot core is expelled which expands and surrounds a cooler region moved inwards. Fast ions conforming to this model would give a neutron emission profile similar to that shown in Fig. 8 with the addition of an axial contribution from ions injected after the sawtooth crash. The exact amount of the expected axial contribution has not been calculated, since the beam slowing down distribution is very far from equilibrium. However, when the beam injection time is much less than a slowing down time, an estimate is obtained from the product of the axial beam source rate, the time of injection after the sawtooth crash, the thermal deuteron density, and the reaction rate at the beam injection energy. This estimate gives an axial beam-plasma neutron emissivity of several times $10^{14} m^{-3} s^{-1}$, which corresponds to the experimental value as deduced by tomography averaged over 10 ms after the sawtooth crash.

The behaviour seen in the sawtooth crash as described above has been seen in several discharges with neutron emission rates of order 10^{16} n/s. At higher rates, the analysis is somewhat less accurate for the reasons described in the E_t/E_f discussion, but interesting because of the broader emissivity profile before the sawtooth crash. In Discharge 20983, similar to Discharge 20981, but with different timing, several sawteeth occur, including one at 10.489 s with a higher neutron global neutron emission rate of 2.4×10^{16} n/s. The ion temperature is higher at 21 kev, resulting in a larger contribution to the neutron emission from thermal and beam-plasma sources. The emission profile before the sawtooth crash is relatively broad, with a FWHM of 0.8 m. The sawtooth crash causes a drop in global neutron emission of 12%, and the profile after the sawtooth crash has a FWHM of 1.2 m with a hollow profile, with a maximum emissivity about half that of the profile before the sawtooth. The electron temperature profile is relatively flat between the major radii of 2.9 and 3.6 m before the sawtooth crash and has widened to 2.8 to 3.7 m after it. The major radius at which sawtooth inversion is observed on the electron temperature is 3.6 m. Comparing the sawteeth in Discharges 20981 and 20983, the width of the emissivity profiles is similar after the sawtooth crash, even with very different pre-crash widths. The relative drop in maximum emissivity is greater for the more initially peaked profile.

Sawteeth with larger relative drops in global neutron emission than in the discharges discussed above are observed at the beta limit as discussed by SMEULDERS et al. (1990). Discharge 20881 is a mostly hydrogen plasma with 5.5% toroidal beta, heated by deuterium beams, so the axial neutron emissivity before a sawtooth at 14.36 s is only $5 \times 10^{13} m^{-3} s^{-1}$. The global emission is $6 \times 10^{14} s^{-1}$ for which the neutron camera requires an integration time of 100 ms, about equal to the beam slowing-down time of 80 ms. The axial contributions are 1/2 bb and 1/2 bp. A ratio of deuteron-to-electron density of only 1/6 is required for consistency with the total emissivity. The sawtooth crash results in a fall of the global emission to 2/3 of its previous value. The emissivity profile broadens, with axial emissivity only 1/3 of the pre-crash value. Given the limitations imposed by the long sampling time, the behaviour of the emissivity profiles and the physics seem similar to the high emissivity case.

To conclude the discussion of sawteeth, we further observe that large amplitude sawtooth crashes also occur in both global neutron

emission and emissivity profiles of discharges produced either by ohmic heating alone, or by ion cyclotron radio frequency heating on JET. Since such discharges (with the exception of deuterium heating by RF as shown by SADLER et al. (1990b)) are dominated by thermal emission, they are not considered in detail in this paper, but will be the subject of future investigations.

4. CONCLUSIONS

For low and medium density plasmas without sawteeth, neutron emissivity profiles are observed to be peaked. The width depends on neutral beam deposition, plasma profiles and emission sources. A sawtooth crash causes the neutron emissivity and particularly the beam-beam component to collapse on axis. The drops in global neutron emission at sawtooth crashes are typically smaller for plasmas which are dominated by beam-plasma neutron production, and larger when beam-beam production is important. The shape and width of the emissivity profile after a crash are consistent with a model of electron sawteeth (presently used to explain JET results). Neutron emissivity profiles and the effect of a sawtooth crash are observed to depend upon the dominating sources of neutron emission and plasma profiles. At high plasma densities, the emission profile is observed to shift outwards to large major radius. These results show that the analysis of neutron emissivity profiles has importance for the understanding of fast ion distributions, sawteeth, their effects on transport, the optimization of neutron yields for given heating conditions and the extrapolation to neutron yields for reactor-relevant conditions.

REFERENCES

ADAMS, J.M., CHEETHAM, A., CONROY, S., GORINI, G., GOTTARDI, N., IGUCHI, T., JARVIS, O.N., SADLER, G., SMEULDERS, P., WATKINS, N. and VAN BELLE, P. (1989) Proc. 16th EPS Conf. Venice 13B I, 63.

BALET, B., CORDEY, J.G., HEATON, A.D. and STUBBERFIELD, P.M. (1989) APS Conf. Anaheim, JET Preprint JET-P(89)80.

BATISTONI, P., RAPISARDA, M. and ANDERSON, D. (1990) Nucl. Fusion 30(4), 625.

CAMPBELL, D.J., CORDEY, J.G., EDWARDS, A.W., GILL, R.D., LAZZARO, E., MAGYAR, G., McCARTHY, A.L., O'ROURKE, J., PEGORARO, F., PORCELLI, F., SMEULDERS, P., START, D.F.H., STUBBERFIELD, P., WESSON, J.A., WESTERHOF, E. and ZASCHE, D. (1988) Plasma Physics and Controlled Nuclear Fusion (Proc. 12th Int. Conf. Nice), Vol. 1, 377.

CONROY, S.W. (1990) Diagnosis of Fusion Products for Reactor Relevant Plasmas, Ph.D. Thesis, Imperial College, London.

CORE, W.G.F. (1985) A solution of the ICRF Fokker-Planck Equation, JET Preprint JET-P(85)30.

GRANETZ, R.S. and SMEULDERS, P. (1988) Nucl. Fusion 28(3), 457.

JARVIS, O.N., ADAMS, J.M., BALET, B., CONROY, S.W., CORDEY, J.G., ELEVANT, T., GILL, R.D., LOUGHLIN, M.J., MANDL, W., MORGAN, P.D., PASINI, D., SADLER, G., WATKINS, N., VAN BELLE, P., VON HELLERMAN, M. and WEISEN, H. (1990) Nucl. Fusion 30(2), 307.

LOUGHLIN, M. J., ADAMS, J.M., HAWKES, N., HONE, M., JARVIS, O.N., LAUNDY, B., SADLER, G., SYME, D.B., WATKINS, N. and VAN BELLE, P. (1989) Proc. 16th EPS Conf. Venice, 13B I, 83.

LOVBERG, J.A., HEIDBRINK, W.W., STRACHAN, J.D. and ZAVERYAEV, V.S. (1989) Phys. Fluids B 1(4), 874.

MARCUS, F.B., PFEIFFER, W., ARMENTROUT, C.J., HARVEY, R.W., JAHNS, G.L., PETRIE, T.W. and ZAWADZKI, E. (1983) Giant Sawtooth Oscillations in the Doublet III Tokamak. GA Technologies Report GA-A16960, San Diego.

PFEIFFER, W., MARCUS, F.B., ARMENTROUT, C.J., JAHNS, G.L., PETRIE, T.W. and STOCKDALE, R.E. (1985) Nucl. Fusion 25(6), 655.

SADLER, G., CONROY, S., JARVIS, O.N., VAN BELLE, P., ADAMS, J.M., and HONE, M. (1989) IAEA Conf. Kiev, JET Preprint JET-P(89)77.

SADLER, G. et al. (1990a) D-D Fusion Reactivity studies in high temperature JET Plasmas. JET Preprint JET-P(90)10, Submitted to Nucl. Fusion.

SADLER, G., et al. (1990b) Proc. 17th EPS Conf. Amsterdam 14B I,1.

SMEULDERS, P., ADAMS, J.M., BALET, B., CAMPBELL, D., CHEETHAM, A., CORTI, S., EDWARDS, A., GOTTARDI, N., GOWERS, C., HENDER, T.C., HUYSMANS, G., JACQUINOT, J., JOFFRIN, E., KWON, O., LAZZARO, E., MARCUS, F.B., MORGAN, P., NAVE, F., NIELSEN, P., O'BRIEN, D., O'ROURKE, J., PORCELLI, F., PORTE, L., SADLER, G., SIPS, G., START, D., TANGA, A., WARD, D. and WEISEN, H. (1990) Proc. 17th EPS Conf. Amsterdam, 14B I, 323.

VAN BELLE, P. AND SADLER, G. (1986) in Basic and Advanced Diagnostic Techniques for Fusion Plasmas, Varenna, Vol. III, EUR 10797 EN.

ACKNOWLEDGEMENTS

We gratefully acknowledge and thank D Campbell, R Gill, M F F Nave, P. Stott, and P Stubberfield for data, programs, and useful discussions.

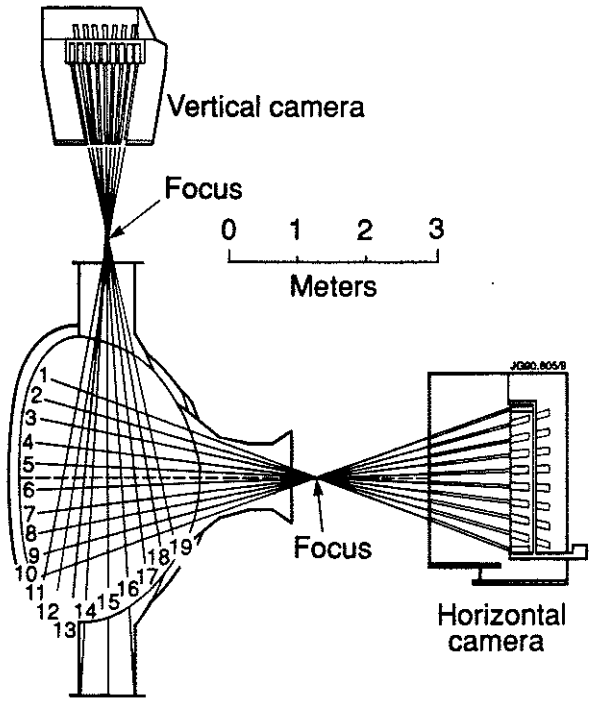

Fig. 1. JET neutron profile monitor and detector lines-of-sight.

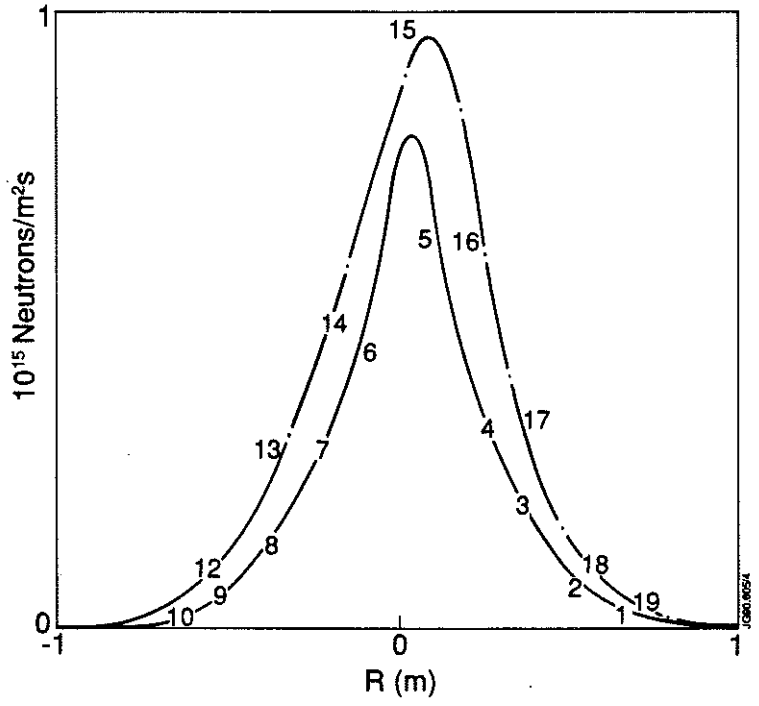

Fig. 2. Comparison of measured channel data (numbers) from 2 neutron cameras and line-integrals (the solid and dashed curves are the vertical and horizontal cameras, respectively) recalculated from emissivity profiles deduced by tomography (time-integrated from 10.738 to 10.748 s) versus major radius of intersection with the ellipse tangent to the channel. Shown for Discharge 20981 from 10.738 to 10.748 s.

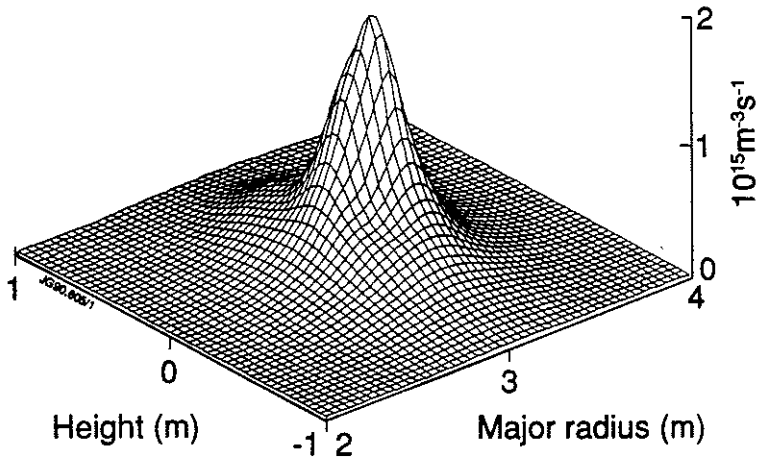

Fig. 3. Neutron emissivity profile before the sawtooth crash (time integrated from 10.738 to 10.748 s) versus major radius and vertical height for Discharge 20981.

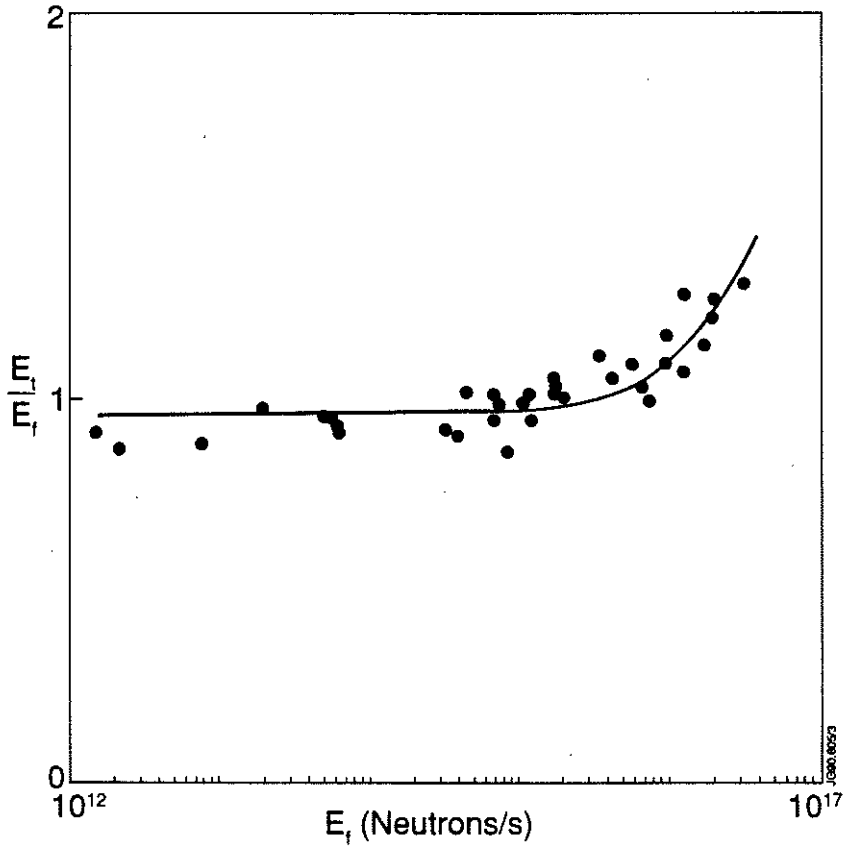

Fig. 4. Ratio of E_t (the global neutron emission from integration over emissivity profiles) to E_f (the global neutron emission from fission chamber measurements) versus global neutron emission, and a linear fit.

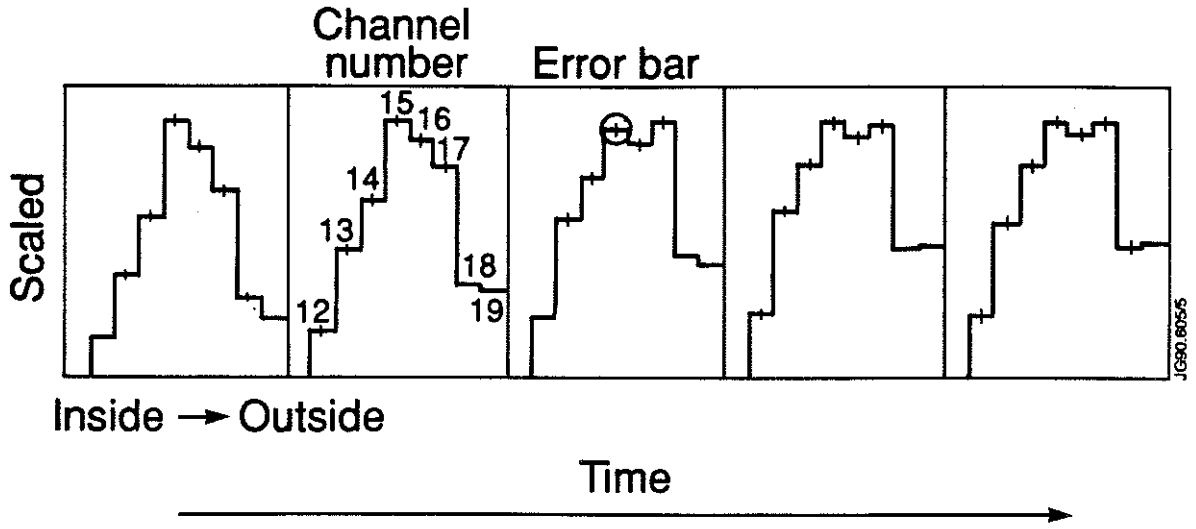

Fig. 5. Measured line-integral emission from the vertical camera channels for successive 1 s bins (10 - 11 s to 14 - 15 s), scaled for Discharge 21022, a long-pulse H-mode where the electron density increases with time.

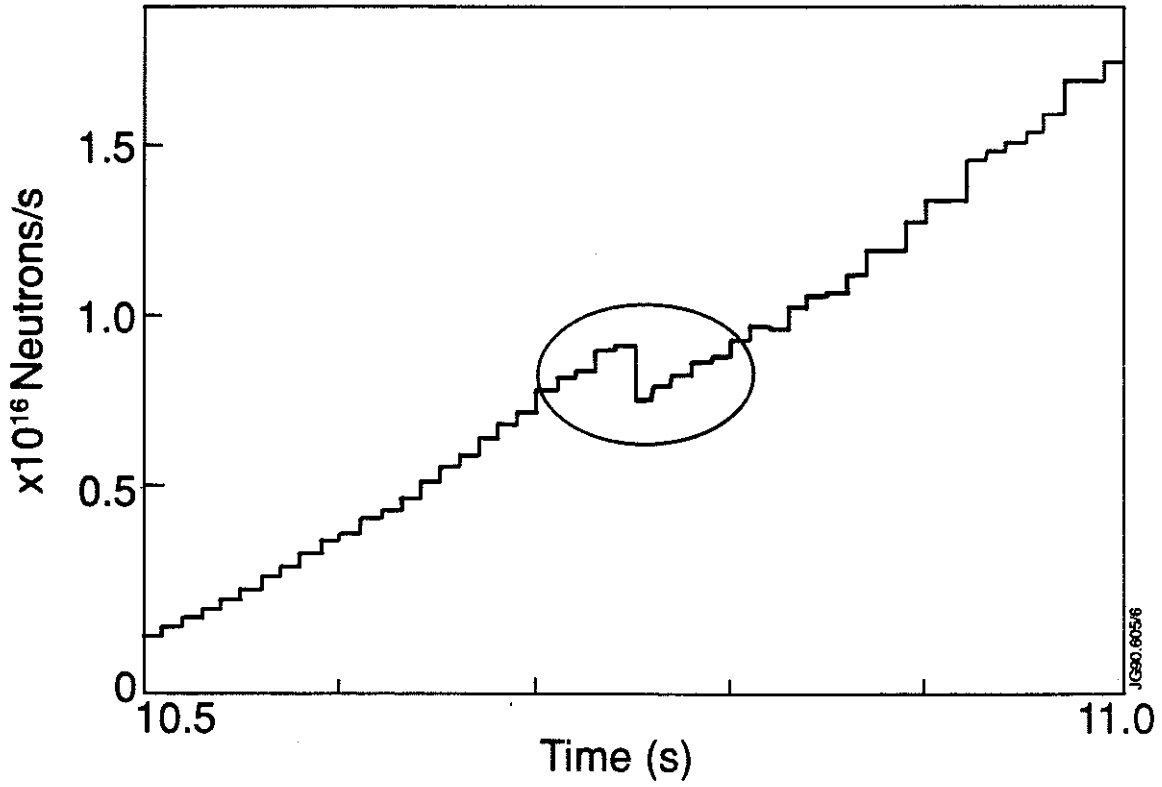

Fig. 6. Global neutron emission versus time, showing a sawtooth at 10.75 s for Discharge 20981.

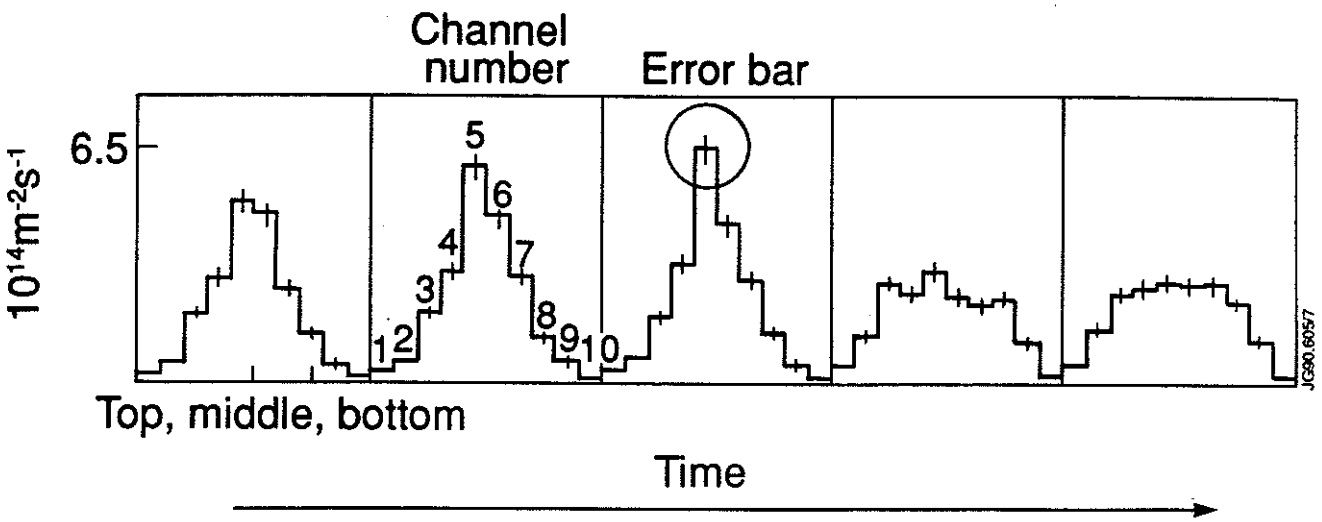

Fig. 7. Measured line-integral emission from 10 horizontal camera channels for successive 10 ms time bins (10.72 - 10.73 s to 10.76 - 10.77 s) for Discharge 20981.

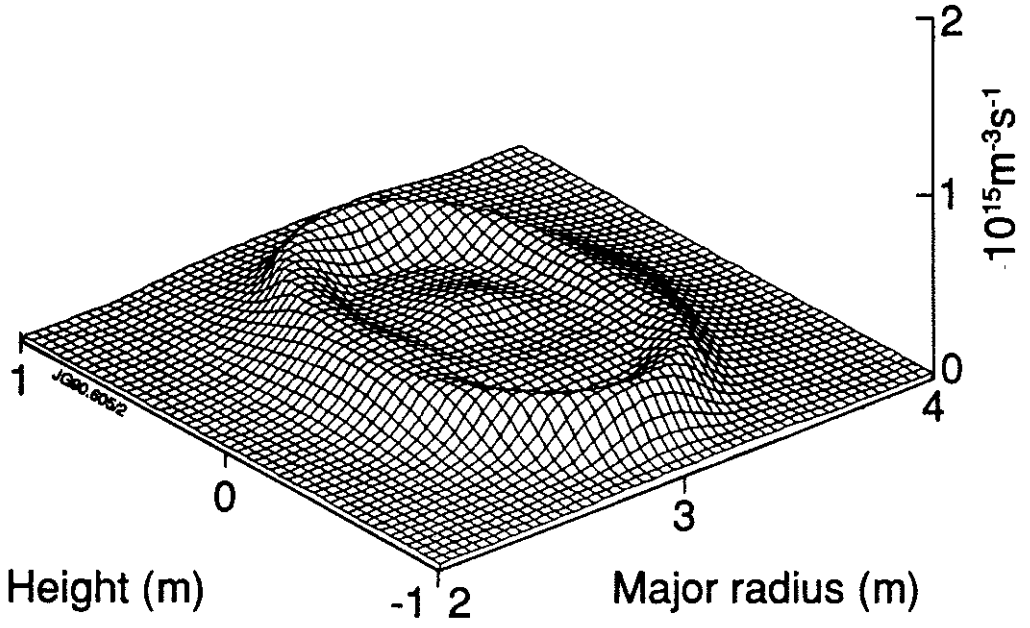

Fig. 8. Neutron emissivity profile after the sawtooth crash (time integrated from 10.756 - 10.766 s) versus major radius and vertical height for Discharge 20981.

APPENDIX 1.

THE JET TEAM

JET Joint Undertaking, Abingdon, Oxon, OX14 3EA, U.K.

J.M.Adams[1], F.Alladio[4], H.Altmann, R.J.Anderson, G.Appruzzese, W.Bailey, B.Balet, D.V.Bartlett, L.R.Baylor[24], K.Behringer, A.C.Bell, P.Bertoldi, E.Bertolini, V.Bhatnagar, R.J.Bickerton, A.Boileau[3], T.Bonicelli, S.J.Booth, G.Bosia, M.Botman, D.Boyd[31], H.Brelen, H.Brinkschulte, M.Brusati, T.Budd, M.Bures, T.Businaro[4], H.Buttgereit, D.Cacaut, C.Caldwell-Nichols, D.J.Campbell, P.Card, J.Carwardine, G.Celentano, P.Chabert[27], C.D.Challis, A.Cheetham, J.Christiansen, C.Christodoulopoulos, P.Chuilon, R.Claesen, S.Clement[30], J.P.Coad, P.Colestock[6], S.Conroy[13], M.Cooke, S.Cooper, J.G.Cordey, W.Core, S.Corti, A.E.Costley, G.Cottrell, M.Cox[7], P.Cripwell[13], F.Crisanti[4], D.Cross, H.de Blank[16], J.de Haas[16], L.de Kock, E.Deksnis, G.B.Denne, G.Deschamps, G.Devillars, K.J.Dietz, J.Dobbing, S.E.Dorling, P.G.Doyle, D.F.Düchs, H.Duquenoy, A.Edwards, J.Ehrenberg[14], T.Elevant[12], W.Engelhardt, S.K.Erents[7], L.G.Eriksonn[5], M.Evrard[2], H.Falter, D.Flory, M.Forrest[7], C.Froger, K.Fullard, M.Gadeberg[11], A.Galetsas, R.Galvao[8], A.Gibson, R.D.Gill, A.Gondhalekar, C.Gordon, G.Gorini, C.Gormezano, N.A.Gottardi, C.Gowers, B.J.Green, F.S.Griph, M.Gryzinski[26], R.Haange, G.Hammett[6], W.Han[9], C.J.Hancock, P.J.Harbour, N.C.Hawkes[7], P.Haynes[7], T.Hellsten, J.L.Hemmerich, R.Hemsworth, R.F.Herzog, K.Hirsch[14], J.Hoekzema, W.A.Houlberg[24], J.How, M.Huart, A.Hubbard, T.P.Hughes[32], M.Hugon, M.Huguet, J.Jacquinot, O.N.Jarvis, T.C.Jernigan[24], E.Joffrin, E.M.Jones, L.P.D.F.Jones, T.T.C.Jones, J.Källne, A.Kaye, B.E.Keen, M.Keilhacker, G.J.Kelly, A.Khare[15], S.Knowlton, A.Konstantellos, M.Kovanen[21], P.Kupschus, P.Lallia, J.R.Last, L.Lauro-Taroni, M.Laux[33], K.Lawson[7], E.Lazzaro, M.Lennholm, X.Litaudon, P.Lomas, M.Lorentz-Gottardi[2], C.Lowry, G.Magyar, D.Maisonnier, M.Malacarne, V.Marchese, P.Massmann, L.McCarthy[28], G.McCracken[7], P.Mendonca, P.Meriguet, P.Micozzi[4], S.F.Mills, P.Millward, S.L.Milora[24], A.Moissonnier, P.L.Mondino, D.Moreau[17], P.Morgan, H.Morsi[14], G.Murphy, M.F.Nave, M.Newman, L.Nickesson, P.Nielsen, P.Noll, W.Obert, D.O'Brien, J.O'Rourke, M.G.Pacco-Düchs, M.Pain, S.Papastergiou, D.Pasini[20], M.Paume[27], N.Peacock[7], D.Pearson[13], F.Pegoraro, M.Pick, S.Pitcher[7], J.Plancoulaine, J-P.Poffé, F.Porcelli, R.Prentice, T.Raimondi, J.Ramette[17], J.M.Rax[27], C.Raymond, P-H.Rebut, J.Removille, F.Rimini, D.Robinson[7], A.Rolfe, R.T.Ross, L.Rossi, G.Rupprecht[14], R.Rushton, P.Rutter, H.C.Sack, G.Sadler, N.Salmon[13], H.Salzmann[14], A.Santagiustina, D.Schissel[25], P.H.Schild, M.Schmid, G.Schmidt[6], R.L.Shaw, A.Sibley, R.Simonini, J.Sips[16], P.Smeulders, J.Snipes, S.Sommers, L.Sonnerup, K.Sonnenberg, M.Stamp, P.Stangeby[19], D.Start, C.A.Steed, D.Stork, P.E.Stott, T.E.Stringer, D.Stubberfield, T.Sugie[18], D.Summers, H.Summers[20], J.Taboda-Duarte[22], J.Tagle[30], H.Tamnen, A.Tanga, A.Taroni, C.Tebaldi[23], A.Tesini, P.R.Thomas, E.Thompson, K.Thomsen[11], P.Trevalion, M.Tschudin, B.Tubbing, K.Uchino[29], E.Usselmann, H.van der Beken, M.von Hellermann, T.Wade, C.Walker, B.A.Wallander, M.Walravens, K.Walter, D.Ward, M.L.Watkins, J.Wesson, D.H.Wheeler, J.Wilks, U.Willen[12], D.Wilson, T.Winkel, C.Woodward, M.Wykes, I.D.Young, L.Zannelli, M.Zarnstorff[6], D.Zasche[14], J.W.Zwart.

PERMANENT ADDRESS

1. UKAEA, Harwell, Oxon. UK.
2. EUR-EB Association, LPP-ERM/KMS, B-1040 Brussels, Belgium.
3. Institute National des Récherches Scientifique, Quebec, Canada.
4. ENEA-CENTRO Di Frascati, I-00044 Frascati, Roma, Italy.
5. Chalmers University of Technology, Göteborg, Sweden.
6. Princeton Plasma Physics Laboratory, New Jersey, USA.
7. UKAEA Culham Laboratory, Abingdon, Oxon. UK.
8. Plasma Physics Laboratory, Space Research Institute, Sao José dos Campos, Brazil.
9. Institute of Mathematics, University of Oxford, UK.
10. CRPP/EPFL, 21 Avenue des Bains, CH-1007 Lausanne, Switzerland.
11. Risø National Laboratory, DK-4000 Roskilde, Denmark.
12. Swedish Energy Research Commission, S-10072 Stockholm, Sweden.
13. Imperial College of Science and Technology, University of London, UK.
14. Max Planck Institut für Plasmaphysik, D-8046 Garching bei München, FRG.
15. Institute for Plasma Research, Gandhinagar Bhat Gujat, India.
16. FOM Instituut voor Plasmafysica, 3430 Be Nieuwegein, The Netherlands.
17. Commissiariat à L'Energie Atomique, F-92260 Fontenay-aux-Roses, France.
18. JAERI, Tokai Research Establishment, Tokai-Mura, Naka-Gun, Japan.
19. Institute for Aerospace Studies, University of Toronto, Downsview, Ontario, Canada.
20. University of Strathclyde, Glasgow, G4 ONG, U.K.
21. Nuclear Engineering Laboratory, Lapeenranta University, Finland.
22. JNICT, Lisboa, Portugal.
23. Department of Mathematics, Univeristy of Bologna, Italy.
24. Oak Ridge National Laboratory, Oak Ridge, Tenn., USA.
25. G.A. Technologies, San Diego, California, USA.
26. Institute for Nuclear Studies, Swierk, Poland.
27. Commissiariat à l'Energie Atomique, Cadarache, France.
28. School of Physical Sciences, Flinders University of South Australia, South Australia SO42.
29. Kyushi University, Kasagu Fukuoka, Japan.
30. Centro de Investigaciones Energeticas Medioambientales y Techalogicas, Spain.
31. University of Maryland, College Park, Maryland, USA.
32. University of Essex, Colchester, UK.
33. Akademie de Wissenschaften, Berlin, DDR.

CR 88.49.1A